PCCP

PAPER

View Article Online
View Journal | View Issue

Cite this: *Phys. Chem. Chem. Phys.*, 2019, **21**, 3683

Algebraic diagrammatic construction for the polarisation propagator in combination with effective fragment potentials†

Reena Sen,[a] Andreas Dreuw *[a] and Shirin Faraji *[b]

Received 19th October 2018,
Accepted 18th December 2018

DOI: 10.1039/c8cp06527f

rsc.li/pccp

The effective fragment potential (EFP) method for the efficient inclusion of solvation effects is combined with the algebraic diagrammatic construction (ADC) scheme for the second- and third-order polarisation propagator. The accuracy of these newly developed EFP-ADC(2) and EFP-ADC(3) methods is tested with respect to supermolecular ADC calculations for a selected set of small solute·solvent complexes. The EFP model for solvation introduces only marginal errors in the excitation energies and oscillator strengths of singlet as well as triplet states, which are strictly localized on the chromophore, significantly below the intrinsic errors of the parent ADC(2) and ADC(3) methods. It is only when delocalization of electron density on the solvent molecules occurs that the error in the excitation energies increases, a well-known behavior of environment models in general. Overall, EFP-ADC schemes prove to be reliable computational approaches to simulate electronic absorption spectra in solution.

1 Introduction

Inclusion of the effect of a solvent on a chromophore or photoactive molecule is critically important for the theoretical description of photochemical and photophysical phenomena in solution. Since the full quantum mechanical description of the complete solute–solvent system is computationally generally not feasible due to the steep computational scaling of electronic structure methods,[1] various solvation models exist to be used within quantum chemical calculations. In such calculations, the investigated system is separated into the molecule of interest, which is calculated with some high-level quantum chemical method, and the environment, which is modelled at a lower level of quantum chemistry or using classical theories. Solvation models are generally distinguished as implicit and explicit ones.

For an implicit treatment, continuum solvation models such as polarisable continuum models (PCMs)[2–4] and, in particular, the conductor-like screening model (COSMO)[5] are widely used. In these models, the environment is treated classically as a polarisable continuum incorporating solvent effects by considering bulk physical parameters of the medium such as the dielectric constant and the refractive index. Thereby, sampling of nuclear degrees of freedom is also implicitly taken into account. Hence, continuum models thus provide free energies of solvation. They are particularly well suited for modelling isotropic environments like molecules in weakly interacting solvents, in which electrostatic interactions dominate.

In explicit solvation models, the environment is generally described with atomic resolution, which is particularly useful for anisotropic molecular systems and when the chemistry is driven by specific key solute–solvent interactions. This is, for example, the case in typical quantum mechanical/molecular mechanical (QM/MM) schemes,[6] in which the point-charge distribution of the environment is taken into account, which is referred to as electrostatic embedding. Usually, the point charges are taken from an empirical force-field and are often too large, compensating for missing polarisation, because such parameters are rarely intended to reproduce the microscopic detail required for accurate embedding calculations. In general, the empirical nature of MM force-fields limits their predictive power.

In contrast, the polarisable embedding (PE) model[7,8] is a fragment based, hybrid quantum-classical embedding scheme. The required parameters are obtained from quantum chemical calculations of small split fragments of the molecular environment. The charge distribution of the environment is modelled by fragment-based multicenter multipole expansions and polarisation effects are taken into account by dipole–dipole polarisabilities placed at the multipole expansion sites. PE is generally capable of treating mutual polarisation of the environment and the quantum region and it has been designed

[a] *Interdisciplinary Center for Scientific Computing, Im Neuenheimer Feld 205, 69120 Heidelberg, Germany. E-mail: dreuw@uni-heidelberg.de*
[b] *Zernike Institute for Advanced Materials, Nijenborgh 4, Groningen 9747 AG, The Netherlands*

† Electronic supplementary information (ESI) available. See DOI: 10.1039/c8cp06527f

to obtain accurate molecular response properties, *e.g.*, electronic excitation energies.

The effective fragment potential (EFP)[9,10] method is closely related to PE embedding and the description of electrostatics and polarisation is nearly identical, and for modelling intermolecular interactions, similar strategies based on multipolar expansions have been utilised.[11–13] However, EFP features a more rigorous treatment of dispersion and exchange repulsion. The EFP method is free from any fitted parameters and owing to its construction, free from basis set superposition error. The method was first introduced for the theoretical description of biological molecules in large water clusters (EFP1),[14,15] and later extended to other solvents (EFP2).[14]

In order to include solvent effects in excited state calculations, the response of the EFP environment to changes in the electronic distribution of the solute needs to be included.[16–19] Existing implementations allow for the combination of EFP with many popular excited-state methods including equation-of-motion coupled cluster (EOM-CC),[20–22] time-dependent density functional theory (TDDFT),[23–25] configuration interaction singles with perturbative doubles (CIS(D)),[26] and spin-opposite-scaled (SOS) CIS(D).[27] Here, we introduce the combination of EFP with the algebraic diagrammatic construction scheme of the second- and third-order polarisation propagator, ADC(2)[28] and ADC(3),[29,30] respectively.

Recently, ADC schemes of the polarisation propagator have attracted considerable attention because of their robustness and reliable accuracy for excitation energies of predominantly singly-excited states.[31,32] Its mathematical formulation based on the intermediate state representation (ISR) allows for the convenient calculation of wave-function based excited state properties.[33] Since ADC schemes are size-consistent, they are well suited to compute properties of large molecular systems.[32] Besides computation of excited-state properties, the ISR approach facilitates interfacing between ADC methods and solvent models represented by one-particle potentials. Following this route, ADC has been employed within classical QM/MM schemes,[34] and it has been interfaced with many other solvent models such as PCM,[35–37] PE[38] and frozen-density embedding (FDE).[39–41]

This paper is organised as follows. In the next section, the basic theoretical concepts of EFP-ADC will be outlined before its accuracy is tested for three different subsets of ''solvated'' molecules. First, representative organic molecules solvated with one single molecule are investigated, then nitrobenzene and coumarin solvated with different solvent molecules are investigated, and finally, the excited states of thymine solvated with one, two, three and five water molecules are studied. In this study, singlet and triplet excited states are first calculated for the isolated molecules in the gas phase and then supermolecular calculation of the molecule–solvent complex is performed at the ADC(2) and ADC(3) levels and afterwards compared to the corresponding EFP-ADC calculations. Overall, the excited states calculated at the EFP-ADC level agree very favourably with the ones obtained at the supermolecular ADC level.

2 Theoretical details

The theoretical details of the EFP method have been described in detail previously,[9,10,17] as well as the theoretical foundations of ADC.[28,29,32,33,42] Here, only the immediately required details for the combination of EFP with ADC will be outlined. In general, it is closely related to the combination of EFP with EOM-CC.[17] EFP-ADC has been included into a development version of Q-Chem 5.0.[43]

Within ADC schemes for the polarisation propagator, the solution of the Hermitian eigenvalue equation

$$\mathbf{MX} = \mathbf{\Omega X}, \quad \mathbf{X}^{\dagger}\mathbf{X} = 1 \tag{1}$$

yields excitation energies ω_n and excited state vectors $\mathbf{x}_n$ as eigenvalues and eigenvectors, respectively. $\mathbf{M}$ corresponds to the Hamiltonian shifted by the ground state energy expressed in the intermediate state (IS) basis for excited states, both obtained at some level of perturbation theory.[33,44] The typical Møller–Plesset partitioning of the Hamiltonian is employed, $\hat{H} = \hat{F} + \hat{U}$, with $\hat{F}$ being the Fock-operator and $\hat{U}$ the fluctuation potential resembling electron correlation. Correspondingly, $\mathbf{M}$ is also a perturbation theoretical expansion and can be written as

$$\mathbf{M} = \mathbf{K} + \mathbf{C}^{(1)} + \mathbf{C}^{(2)} + \cdots \mathbf{C}^{(n)} \tag{2}$$

where $\mathbf{K}$ corresponds to zeroth order, *i.e.* the expectation value of the Fock operator of the zeroth-order intermediate states, the Slater determinants. Hence, $\mathbf{K}$ is diagonal with orbital energy difference between occupied and virtual orbitals. The IS basis is important to note to be orthogonal and uncoupled from the MPn electronic ground state, and therefore, a ground state MP calculation is generally not required to obtain excitation energies, but only a Hartree–Fock (HF) calculation for the required one-particle energies and orbitals. More detailed derivations of the algebraic diagrammatic construction scheme for the polarisation propagator (ADC) are given in the literature.[28,29,32,33,42]

Due to the structure of the ADC matrix (eqn (2)), different pathways for treating external one-particle potentials within ADC arise. On one hand, it can be included in the Fock-operator to obtain perturbed one-particle energies and orbitals and a standard ADC calculation is performed utilising those. On the other hand, the one-particle potential can be represented in the IS basis and added to the ADC matrix after an unperturbed HF calculation has been performed. At approximate ADC levels, both approaches offer advantages, however, to include a one-particle potential at HF level provides fully relaxed orbitals with respect to the potential and only minimal changes to the existing ADC codes need to be made.

Effective fragment potentials are such one-particle potentials, however, with the further complication of depending on the wavefunction of the quantum system, the solute, as well.[9,10] In particular, the induced dipoles on the solvent molecules as well as the polarisation of the solute interdepend on each other. Therefore, a two-level iteration scheme is employed and at each iteration of the HF cycle, the induced dipoles of the effective fragments are iterated until self-consistency with each other and with the current HF determinant is achieved. Once these

EFP-HF equations are converged, the obtained induced dipoles of the solvent are consistent with each other and with the electronic HF ground state of the solute, yielding a suitable EFP one-particle potential to be included in subsequent calculations of the solute "alone", *e.g.* in computationally demanding ground-state correlation methods or excited-state methods. The total energy of the ground state is then given as

$$E_0 = \langle \Psi_0 | \hat{H} + \hat{v}_C + \hat{v}_{pol,0} | \Psi_0 \rangle + E_C^{EFP} + E_{pol,0}^{EFP} + E_{disp}^{EFP/QM} + E_{xrep}^{EFP/QM}, \quad (3)$$

where the expectation on the right hand side of eqn (3) contains the influence of the Coulomb and self-consistent ground state polarisation potentials $\hat{v}_C$ and $\hat{v}_{pol,0}$ in the QM region, while E_C^{EFP} and $E_{pol,0}^{EFP}$ are the electrostatic and polarisation energies of the EFP region, and $E_{disp}^{EFP/QM}$ and $E_{xrep}^{EFP/QM}$ correspond to the dispersion and exchange repulsion energies of both the QM and the EFP region. The details of how these energy contributions are evaluated can be found in ref. 17.

In our current implementation of EFP-ADC, induced dipoles of the fragments are kept unchanged, neither re-adjusted self-consistently at the MP level nor in a state-dependent manner for the ADC excited states, as would be rigorously required. In other words, standard ADC calculations are performed using EFP polarized orbitals and orbital energies. This treatment is, however, an excellent approximation when the HF wave function is a good zeroth-order approximation, which is a general prerequisite for ADC to work well anyway. Nevertheless, at CCSD level, the errors introduced by freezing the induced dipoles at HF level and not relaxing them at CCSD level for the ground state or at the EOM-CCSD level for the excited states have been estimated to be less than 0.001 eV and 0.01 eV for systems with a reasonable HF reference, respectively.[17] However, only small solutes surrounded by a small number of solvent molecules have been evaluated so far, and it should be extended to large solutes with a large sample of solvent molecules comparing the EFP response at HF and post-HF level. In addition, the dispersion and exchange repulsion interactions between the QM solute and the EFP solvent molecules are treated identically like the EFP-EFP interactions as an additive *a posteriori* correction to the total energy. These contributions are thus independent of the considered electronic state.

As the first step of an EFP-ADC calculation, eqn (1) is solved using the orbital energies and molecular orbitals of a converged EFP-HF calculation keeping the EFP-HF polarisation potential $\hat{v}_{pol,0}^{HF}$ frozen, *i.e.* the induced dipoles corresponding to the EFP-HF ground state wavefunction. The ADC excitation energies after diagonalisation of the ADC matrix contain the influence of the Coloumb $\hat{v}_C$ and polarisation $\hat{v}_{pol,0}^{HF}$ potential *via* the single-particle energies contained in the zeroth-order ADC matrix **K**. All other energy contributions arising from the EFP environment, E_C^{EFP}, $E_{pol,0}^{EFP}$, $E_{disp}^{EFP/QM}$ and $E_{xrep}^{EFP/QM}$ of eqn (3) cancel each other in the excitation energies, since the same Coulomb and polarisation field is employed for the ground and excited state and the last two terms are independent of the electronic state. Note, although the MP2 reference state employing $\hat{v}_C$ and the frozen $\hat{v}_{pol,0}^{HF}$ is never explicitly calculated, it is implicitly subtracted owing to the construction of the ADC matrix.

The second step of an EFP-ADC calculation is the computation of a perturbative state-specific correction of the excitation energies due to the response of the EFP potential, *i.e.* the change of the induced dipoles on the solvent molecules, to the electronic excitation, similar to the cLR method developed for PCM.[45] Therefore, the one-electron density of each excited state serves to compute new induced dipole moments μ_n^k and conjugated induced dipole moments $\bar{\mu}_n^k$ at the EFP sites in a single calculation *a posteriori* and not self-consistently. These are then used to compute the perturbative correction according to

$$\begin{aligned}\Delta\omega_n = &\frac{1}{2}\sum_k \left(\mu_0^k - \mu_n^k\right)\left(F_C^k + F_{nuc}^k\right) \\ &+ \frac{1}{2}\sum_k \left(\bar{\mu}_n^k F_{elec,n}^k - \bar{\mu}_0^k F_{elec,0}^k\right) \\ &+ \frac{1}{2}\sum_k \left(\mu_0^k + \bar{\mu}_0^k - \mu_n^k - \bar{\mu}_n^k\right) F_{elec,n}^k,\end{aligned} \quad (4)$$

where the summation runs over all EFP sites. The final EFP-ADC excitation energy of state n is eventually given as the sum of the excitation energy obtained after the diagonalisation of the EFP-ADC matrix and the perturbative correction $\Delta\omega_n$. The first two terms in eqn (4) describe the difference of the polarisation energy E_{pol}^{EFP} of the QM/EFP system in the excited and ground electronic states, while the last term corresponds to the leading correction to the interaction of the ground-state-optimised induced dipoles with the wave function of the excited state.[17]

An important advantage of the perturbative EFP-ADC scheme is that the excited states are orthogonal to each other since they are computed with the same HF ground-state field of the polarisable environment. As a consequence, transition properties between these states can easily be calculated. This would not be the case if each excited state vector would be computed with respect to its own self-consistent EFP field. In addition, the current EFP implementation can be used with any ADC variant available in Q-Chem, ADC(2) and ADC(3) for excitation energies, the core-valence-separated CVS variants,[46–48] spin-opposite-scaled (SOS) variants,[49] or spin–flip ADC.[50,51] Also, all implemented excited-state properties and transition properties, like dipole moments, spin–orbit couplings,[52] and two-photon absorption cross sections,[53] as well as density-based[54,55] and exciton analyses[56] are readily available.

3 Computational details

The geometries of the selected molecular test systems have been optimised at the MP2/cc-pVTZ level. All calculations are done using pure Cartesian basis functions. Subsequent excited state calculations were done using ADC(2) and ADC(3) for the polarisation propagator with the cc-pVTZ basis set for the first subset of test molecules (Fig. 1) and with the cc-pVDZ basis set for the molecular systems of subsets II and III (Fig. 4 and 7). The five lowest singlet and triplet states of the solute molecules

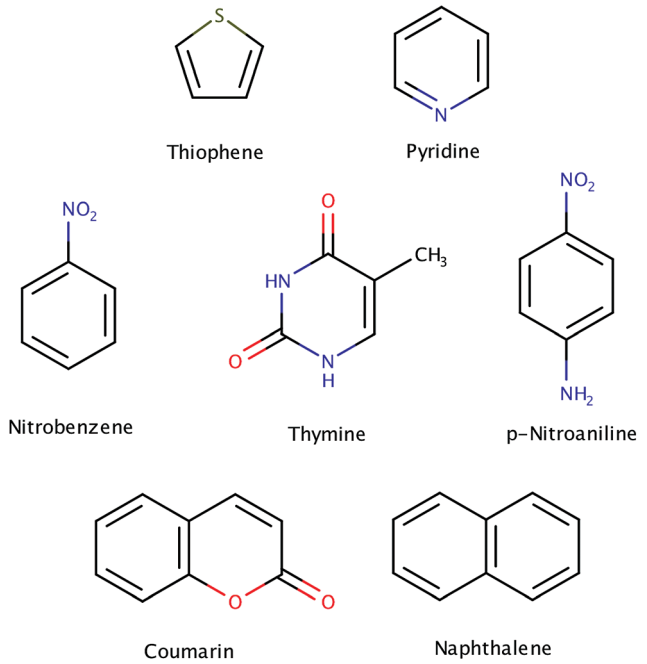

Fig. 1 Subset I of molecules, which are "solvated" with one single water molecule as solvent.

of the test sets are first calculated without solvent isolated in the gas phase, and then the solute–solvent complex in one supermolecular ADC is calculated analogously to obtain the solvent induced shift of the excitation energies. Subsequently, EFP-ADC calculations are conducted describing the solvent molecules as EFPs at Hartree–Fock level and using EFP polarized orbitals and orbital energies. The error with respect to the supermolecular ADC calculations is calculated and analysed. All calculations have been performed with a development version of Q-Chem 5.0 utilising the standard library for effective fragment potentials.[19,43]

4 Performance of EFP-ADC

To test the accuracy of the EFP-ADC methods, three different small test sets of molecular solvent–solute complexes have been selected based on the type of solvent and strength of solute–solvent interaction. The three different subsets are: (i) different organic molecules solvated with one water molecule, (ii) nitrobenzene and coumarin solvated with different single solvent molecules, and (iii) thymine solvated with one, two, three and five water molecules. In the following, the results for these subsets will be briefly described individually and finally jointly statistically evaluated.

4.1 Subset I: different organic chromophores solvated with one water molecule

The seven molecular systems of this subset have been chosen depending on the nature of their interaction with a single water molecule and the feasibility of supermolecular ADC(2) and ADC(3) calculations. The set includes thiophene, pyridine, nitrobenzene, thymine, *p*-nitroaniline, naphthalene, and coumarin as solute and one single water molecule as the "solvent". The geometries are kept the same for the supermolecular ADC(n) calculations and corresponding EFP-ADC(n) calculations. At EFP-ADC(2) level, calculations have been performed for the first five singlet and triplet excited states and the corresponding oscillator strengths (Tables 1 and 2). Altogether, the set comprises 35 singlet excitations and 35 triplet excitations at EFP-ADC(2) level. For EFP-ADC(3), owing to its higher computational effort, the testing has been restricted to only the two smallest systems, *i.e.* thiophene and pyridine (see the ESI†).

Due to the introduction of one explicit water molecule, the order of the first five singlet as well as triplet excited states may change from the isolated gas phase situation. Therefore, a thorough assignment of the states has been performed using

Table 1 Vertical excitation energies and oscillator strengths of the five lowest excited singlet states of the solutes and solute–solvent complexes of subset I computed at ADC(2) level in the gas phase (isolated), at supermolecular ADC(2) level as well as with EFP-ADC(2)

		Excitation energy (eV)			Oscillator strength		
Molecule	State	Isolated	Super-ADC(2)	EFP-ADC(2)	Isolated	Super-ADC(2)	EFP-ADC(2)
Thiophene	S_1	5.835	5.843	5.846	0.0899	0.0859	0.0881
	S_2	6.180	6.172	6.177	0.1120	0.1167	0.1103
	S_3	6.713	6.638	6.688	0.0025	0.0019	0.0022
	S_4	6.777	6.742	6.782	0.0000	0.0000	0.0000
	S_5	7.592	7.579	7.623	0.0000	0.0009	0.0006
Pyridine	S_1	5.053	5.258	5.418	0.0041	0.0033	0.0044
	S_2	5.341	5.610	5.780	0.0000	0.0000	0.0000
	S_3	5.410	5.404	5.407	0.0292	0.0334	0.0349
	S_4	6.792	6.778	6.784	0.0227	0.0148	0.0164
	S_5	7.615	7.618	7.636	0.5911	0.5422	0.5909
Nitrobenzene	S_1	3.694	3.749	3.769	0.0000	0.0000	0.0000
	S_2	4.285	4.340	4.447	0.0002	0.0001	0.0002
	S_3	4.964	4.860	4.862	0.0076	0.0099	0.0100
	S_4	5.561	5.356	5.361	0.2631	0.2973	0.2777
	S_5	5.940	5.911	5.939	0.0839	0.0798	0.0854
Thymine	S_1	4.767	4.804	4.811	0.0000	0.0000	0.0001
	S_2	5.319	5.280	5.255	0.2167	0.2446	0.2266
	S_3	6.187	6.289	6.284	0.0000	0.0000	0.0001
	S_4	6.387	6.477	6.468	0.0676	0.0467	0.0501
	S_5	NA	6.622	6.670	NA	0.2388	0.2627
p-Nitroaniline	S_1	3.746	3.777	3.792	0.0000	0.0000	0.0000
	S_2	4.360	4.453	4.518	0.0002	0.0003	0.0003
	S_3	4.556	4.370	4.381	0.4271	0.4545	0.4352
	S_4	4.769	4.743	4.745	0.0098	0.0078	0.0079
	S_5	5.731	5.638	5.650	0.0004	0.0051	0.0065
Naphthalene	S_1	4.488	4.492	4.507	0.0000	0.0002	0.0004
	S_2	4.841	4.823	4.845	0.0961	0.0913	0.0963
	S_3	6.202	6.159	6.206	0.0000	0.0113	0.0047
	S_4	6.221	6.190	6.239	1.5297	1.4295	1.4804
	S_5	6.296	6.282	6.318	0.0000	0.0050	0.0407
Coumarin	S_1	4.246	4.270	4.265	0.1255	0.1305	0.1326
	S_2	4.503	4.795	4.679	0.0000	0.0000	0.0000
	S_3	5.005	4.998	4.998	0.2005	0.2317	0.2343
	S_4	5.783	5.799	5.799	0.0483	0.0169	0.0159
	S_5	6.176	6.229	6.220	0.5408	0.4957	0.4838

Table 2 Vertical excitation energies and oscillator strengths of the five lowest triplet singlet states of the solutes and solute–solvent complexes of subset I computed at ADC(2) level in the gas phase (isolated), at super-molecular ADC(2) level as well as with EFP-ADC(2)

		Excitation energy (eV)		
Molecule	State	Isolated	Super-ADC(2)	EFP-ADC(2)
Thiophene	T_1	4.116	4.111	4.111
	T_2	4.934	4.958	4.961
	T_3	6.368	6.350	6.349
	T_4	6.449	6.426	6.453
	T_5	6.481	6.417	6.460
Pyridine	T_1	4.519	4.589	4.589
	T_2	4.575	4.772	4.930
	T_3	5.054	5.012	5.012
	T_4	5.304	5.337	5.339
	T_5	5.340	5.568	5.730
Nitrobenzene	T_1	3.443	3.507	3.525
	T_2	3.708	3.750	3.750
	T_3	4.164	4.171	4.185
	T_4	4.694	4.109	4.207
	T_5	4.961	4.586	4.586
Thymine	T_1	3.847	3.853	3.839
	T_2	4.551	4.587	4.597
	T_3	5.460	5.468	5.468
	T_4	6.034	6.161	6.145
	T_5	6.079	6.057	6.044
p-Nitroaniline	T_1	3.507	3.539	3.551
	T_2	3.725	3.625	3.628
	T_3	3.791	3.824	3.824
	T_4	4.130	4.233	4.296
	T_5	4.545	4.541	4.542
Coumarin	T_1	3.294	3.337	3.342
	T_2	4.144	4.136	4.136
	T_3	4.304	4.495	4.606
	T_4	4.521	4.585	4.587
	T_5	4.988	5.061	5.063
Naphthalene	T_1	3.309	3.311	3.315
	T_2	4.357	4.361	4.370
	T_3	4.709	4.698	4.709
	T_4	4.901	4.912	4.930
	T_5	5.008	5.008	5.024

molecular orbitals or even density-based analyses at all levels of theory employed. The absolute error of the shifts corresponds to the difference of the excitation energies. In Table 1, the singlet excitation energies and oscillator strengths of the five lowest singlet excited states and the corresponding oscillator strengths of the molecular subset I are given at ADC(2) level, for the isolated chromophores in the gas phase, including one explicit water molecule in a supermolecular ADC(2) calculation as well as using EFP-ADC(2). The analogous data for the five lowest triplet states are given in Table 2. Since the agreement between the supermolecular ADC(2) and the EFP-ADC(2) values are generally very good, we focus in the following discussion only on the outliers, which exhibit a larger error in the EFP-ADC excitation energies.

In the case of pyridine, the S_1 and S_2 states are observed to possess the largest solvent shifts of 0.205 eV and 0.269 eV and show the largest error of solvatochromic shift of −0.16 eV and −0.17 eV at the level of EFP-ADC(2), respectively. Analysis of the molecular orbitals involved in these two excited states reveals that they possess nπ* character. The molecular orbital corresponding to the lone pair at the nitrogen atom is strongly perturbed due to formation of a hydrogen bond to the water molecule, which leads to a delocalisation of electron density onto the water in the supermolecular ADC(2) calculations (Fig. 2).

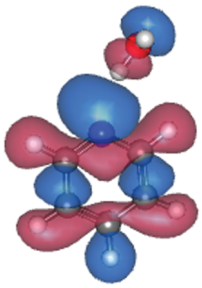

Fig. 2 Representative lone pair *n* orbital of pyridine, which is delocalised over the water solvent molecule. Excitations out of such delocalised orbitals usually exhibit larger errors at EFP-ADC level.

This explains, on one hand, the large solvent-induced shift of the excitation energy, and on the other hand, the large error in the EFP calculation. Such strong interactions leading to electron density delocalisation are simply not well described within the EFP model. The triplet states T_2 and T_5 also correspond to nπ* excited states, and not surprisingly, exhibit the same error at EFP-ADC(2) level. The same effect is seen at the EFP-ADC(3) level as well (ESI†).

The mean signed error (MSE) of the 35 singlet excitation energies for subset I is −0.021 eV with a standard deviation of 0.049 eV, which implies that singlet excitation energies are usually overestimated at EFP-ADC(2) level as compared to supermolecular ADC(2) calculations. The mean absolute error (MAE) for the

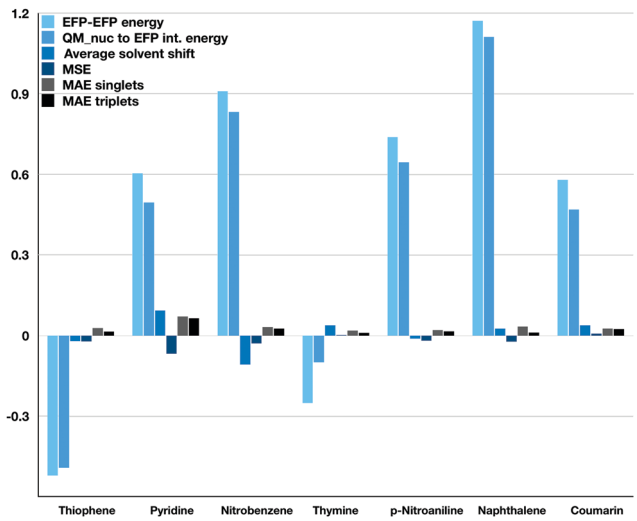

Fig. 3 EFP energy contributions with respect to the QM ground state in Hartree, energy correction for the QM SCF energy due to the EFP; mean solvent shift and MSE for triplet and singlet excitation energies in eV; and MAE for singlet and triplet excitation energies in eV separately for each molecule of subset I.

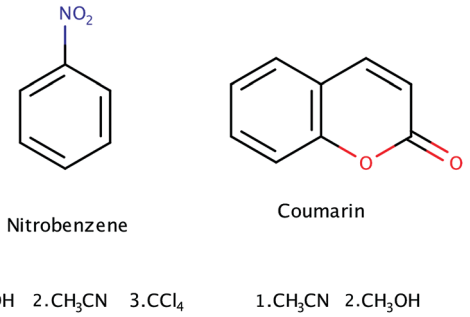

Fig. 4 Molecules in subset II, which are solvated with one molecule of a given solvent.

excitation energies of subset I was found to be 0.031 eV. For oscillator strengths, the accuracy is -0.0029 ± 0.0152. For a deeper analysis of the error contributions, Fig. 3 shows a comparison of the ground-state EFP-EFP energy contributions, the correction of the QM SCF energy due to the EFP, the average solvent shift, MSE for triplet and singlet excitation energies, and the mean solvent shifts. The solvent shift is calculated by subtracting the excitation energies of isolated solutes from the supermolecular ADC(2) energies of solute–solvent complexes to gain a pure quantum mechanical reference value. Pyridine, among all studied systems, has the largest average solvent shift of 0.094 eV and the largest absolute mean errors for both singlets and triplets. Naphthalene and *p*-nitroaniline, on the other hand, are seen to have the strongly repulsive EFP energy contributions of 1.172 Hartree and 0.739 Hartree, respectively, though the MAEs are rather low, which implies that repulsive interactions of the water molecule with the excited states of naphthalene and *p*-nitroaniline are well expressed.

Table 3 Vertical excitation energies and oscillator strengths of the five lowest excited singlet states of the solutes and solute–solvent complexes of subset II computed at ADC(3) level in the gas phase (isolated), at supermolecular ADC(3) level as well as with EFP-ADC(3)

		Excitation energies (eV)			Oscillator strength		
Molecule solvent	State	Isolated	Super-ADC(3)	EFP-ADC(3)	Isolated	Super-ADC(3)	EFP-ADC(3)
Nitrobenzene							
CH_3OH	S_1	4.026	4.070	4.090	0.0000	0.0000	0.0000
	S_2	4.412	4.555	4.583	0.0001	0.0001	0.0001
	S_3	4.831	4.756	4.773	0.0041	0.0066	0.0061
	S_4	5.475	5.366	5.403	0.2364	0.2843	0.2496
	S_5	5.531	5.531	5.533	0.0320	0.0314	0.0348
CH_3CN	S_1	4.026	4.024	3.917	0.0000	0.0000	0.0000
	S_2	4.412	4.475	4.355	0.0001	0.0004	0.0001
	S_3	4.831	4.719	4.816	0.0041	0.0066	0.0040
	S_4	5.475	5.275	5.488	0.2364	0.2543	0.2422
	S_5	5.531	5.506	5.411	0.0320	0.0322	0.0339
CCl_4	S_1	4.026	3.987	3.989	0.0000	0.0009	0.0009
	S_2	4.412	4.369	4.374	0.0001	0.0001	0.0001
	S_3	4.831	4.765	4.783	0.0041	0.0040	0.0041
	S_4	5.475	5.410	5.415	0.2364	0.1989	0.2345
	S_5	5.531	5.441	5.484	0.0320	0.0334	0.0308
Coumarin							
CH_3OH	S_1	4.326	4.360	4.365	0.1138	0.1119	0.1161
	S_2	5.002	5.000	5.010	0.1909	0.2105	0.2164
	S_3	5.054	5.157	5.155	0.0001	0.0001	0.0001
	S_4	5.754	5.826	5.828	0.0222	0.0192	0.0202
	S_5	6.020	6.033	6.049	0.0560	0.0470	0.0409
CH_3CN	S_1	4.326	4.341	4.346	0.1138	0.1104	0.1175
	S_2	5.002	4.985	4.999	0.1909	0.2129	0.2196
	S_3	5.054	5.240	5.188	0.0001	0.0002	0.0001
	S_4	5.754	5.858	5.844	0.0222	0.0250	0.0248
	S_5	6.020	6.004	6.015	0.0560	0.0247	0.0244

4.2 Subset II: nitrobenzene and coumarin with different solvents

In subset II of the selected test molecules (Fig. 4), the errors in the solvatochromic shifts of the excitation energies and oscillator strengths of nitrobenzene and coumarin are analysed in the presence of different single solvent molecules at the EFP-ADC(2) and EFP-ADC(3) level.

For that objective, MP2 optimised molecular geometries of the solute and the solute–solvent complexes are used and the excited electronic states are calculated at the ADC(2), ADC(3), as well as EFP-ADC(2) and EFP-ADC(3) levels using the cc-pVDZ basis set. For nitrobenzene, single solvent molecules of acetonitrile, methanol and chloroform are included, while coumarin is simulated in the presence of acetonitrile and methanol molecules. This test set comprises a total of 30 singlet and triplet excited states. In the following section, the focus lies on the ADC(3) level; corresponding data at the ADC(2) level can be found in the ESI.†

In Table 3, the data for the five lowest excited singlet states of nitrobenzene and coumarin at ADC(3) level are compiled. The overall agreement between the results for the excitation energies and oscillator strengths obtained at supermolecular ADC(3) and EFP-ADC(3) levels is very good. The only larger deviations of EFP-ADC(3) from supermolecular ADC(3) of about 0.1 eV are found for all excited singlet states of the nitrobenzene–acetonitrile solute–solvent complex. Again, a delocalisation of

Table 4 Vertical excitation energies of the five lowest excited triplet states of the nitrobenzene–solvent complexes computed at ADC(3) level in the gas phase (isolated), at supermolecular ADC(3) level and with EFP-ADC(3)

		Excitation energy (eV)		
Molecule solvent	State	Isolated	Super-ADC(3)	EFP-ADC(3)
Nitrobenzene				
CH_3CN	T_1	3.164	3.216	3.214
	T_2	3.716	3.714	3.724
	T_3	3.765	3.755	3.779
	T_4	4.153	4.296	4.322
	T_5	4.422	4.337	4.355
CH_3CN	T_1	3.164	3.219	3.109
	T_2	3.716	3.660	3.607
	T_3	3.765	3.716	3.756
	T_4	4.153	4.215	4.099
	T_5	4.422	4.306	4.406
CCl_4	T_1	3.164	3.122	3.126
	T_2	3.716	3.617	3.625
	T_3	3.765	3.762	3.766
	T_4	4.153	4.110	4.115
	T_5	4.422	4.354	4.378

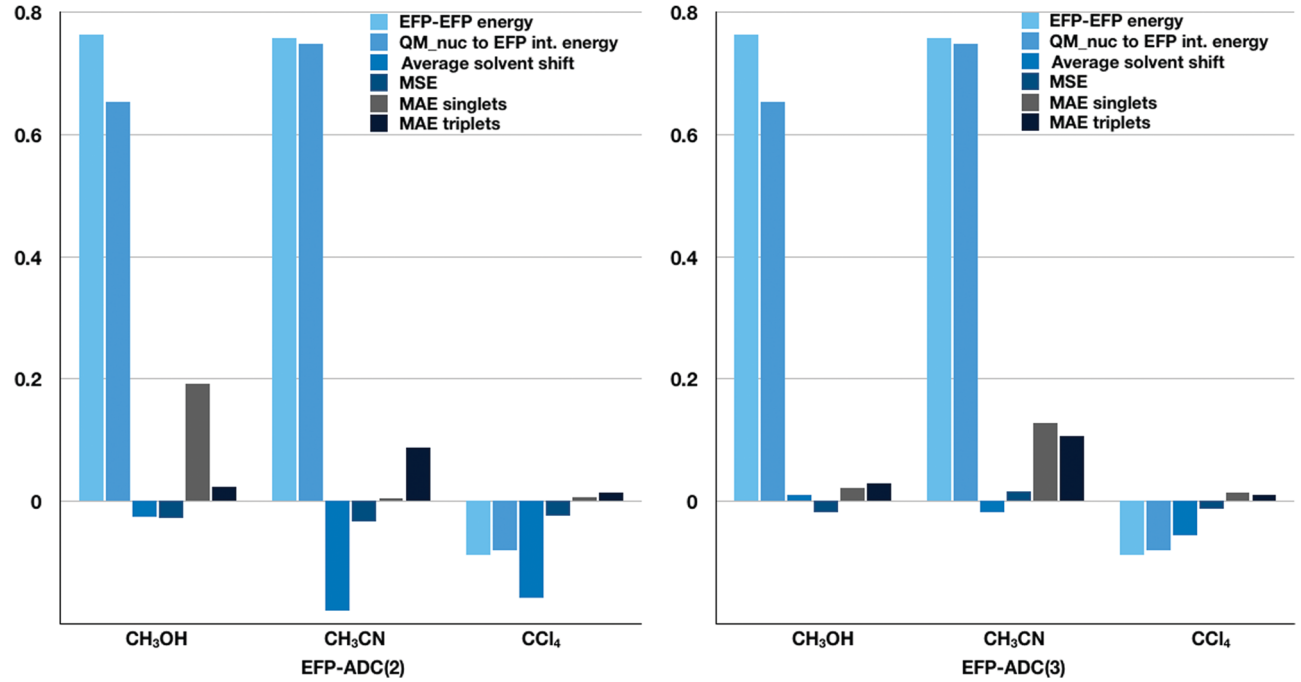

Fig. 5 EFP energy contributions with respect to the QM ground state in Hartree; mean solvent shift and MSE for triplet and singlet excitation energies in eV; and MAE for singlet and triplet excitation energies in eV separately for solvated nitrobenzene: the left plot is for the performance of EFP-ADC(2) and the right plot is for EFP-ADC(3).

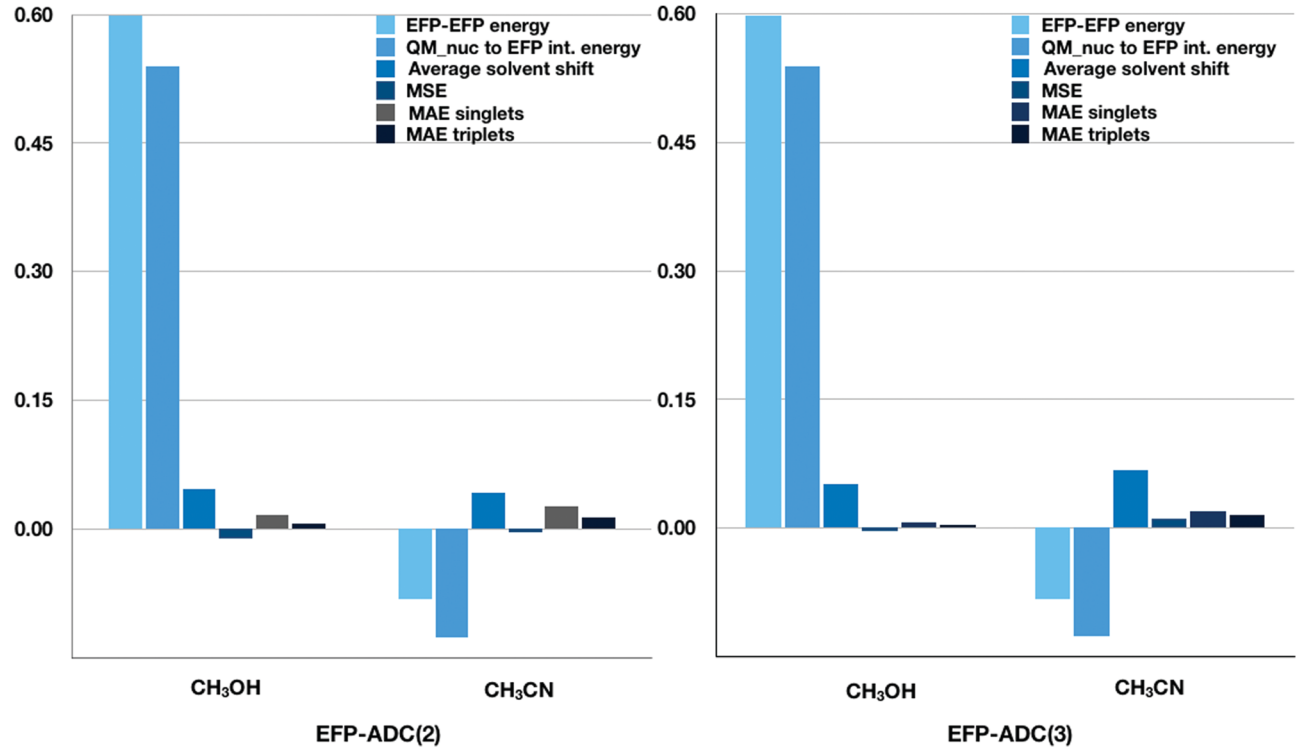

Fig. 6 EFP energy contributions with respect to the QM ground state in Hartree; mean solvent shift and MSE for triplet and singlet excitation energies in eV; and MAE for singlet and triplet excitation energies in eV separately for coumarin: the left plot is for the performance of EFP-ADC(2) and the right plot is for EFP-ADC(3).

the involved occupied orbitals onto the acetonitrile can be identified as the reason for these slightly larger errors. The excitation energies obtained at supermolecular ADC(2) and EFP-ADC(2) levels behave essentially identically (ESI†).

Inspecting the deviations in the triplet excitation energies at EFP-ADC(3) level (Table 4), it becomes apparent that the agreement between supermolecular ADC(3) and EFP-ADC(3) calculations is even better than for the singlet states. Also, for the previously problematic case of the nitrobenzene–acetonitrile complex, the agreement is slightly improved as the deviations are smaller for the triplet states. Seemingly, orbital delocalisation has a smaller effect on triplet states than on singlet states.

It is instructive to relate the magnitude and the character of the EFP-quantum region interaction to the observed errors (Fig. 5). Among the tested solvents, CH_3OH and CH_3CN are seen to have large repulsive EFP-energy contributions to the electronic ground state of nitrobenzene of almost 0.8 Hartree. For water, this EFP ground state energy contribution is even more repulsive with 0.9 Hartree (Table 3). For CCl_4, this contribution is much smaller and attractive by 0.1 Hartree. The magnitude of the EFP-quantum region interaction energy is a direct measure for the interaction strength of the solvent molecule with nitrobenzene, and in general, the stronger the interaction, the larger the solvent shifts of the excitation energies, and the larger the absolute errors.

The solvent shifts observed for the excited states of coumarin are simulated in the presence of molecules of tetrachloromethane and methanol at EFP-ADC(2) and EFP-ADC(3) levels, respectively. The data for the five lowest excited singlet states of coumarin at ADC(3) level are compiled in Table 3. In general, the excitation energies computed at the EFP-ADC(3) level agree very favourably with those obtained at the supermolecular ADC(3) level (Fig. 6), and the maximum deviation is as small as 0.06 eV.

4.3 Thymine solvated with *n* water molecules (*n* = 1, 2, 3, and 5)

For the third subset of the test, the nucleobase thymine was chosen as the solute molecule solvated with up to five water molecules (Fig. 7), since it possesses two hydrogen-bond donor sites and two hydrogen-bond acceptor sites, which provides a large solute–solvent interaction range. The solvent shift of the first five singlet and triplet states in response to solvation with one to five water molecules is analysed following precisely the same procedure as in the previous Section 4.2.

For the thymine·water clusters with one, two, three and five water molecules, the first five excited singlet and triplet states have been calculated comprising n → π* as well as π → π* excited states. As the interaction strength increases with the number of water molecules, the order of the excited states may vary when one water molecule is added. In Tables 5 and 6, the vertical excitation energies and oscillator strengths for singlet and triplet states, respectively, obtained at supermolecular ADC(3) and EFP-ADC(3) levels are compiled together with the main orbital contributions to the transitions. The frontier molecular orbitals are displayed in Fig. S1 of the ESI.† Since the order of states varies with increasing number of water molecules, the leading orbital transitions are also shown for all states. Many excited states, however, possess more than one dominant orbital transition, thus, the given orbital transitions serve only as the orientation, while the assignment has been made based upon careful analysis of the transition densities. The same data obtained at the ADC(2) level can also be found in the ESI† as well. The numbering scheme of the excited states refers to the supermolecular ADC level, *i.e.* the S_i excited state in thymine + $3H_2O$, for example, is the *i*th excited state at the supermolecular ADC level.

Overall, the agreement between the values for the excitation energies of the five lowest singlet and triplet states of the thymine·water complexes obtained at supermolecular ADC(3) and EFP-ADC(3) levels is remarkable. The largest deviation observed is 0.099 eV for the S_2 state of thymine·$3H_2O$. All other computed excitation energies exhibit a much smaller deviation.

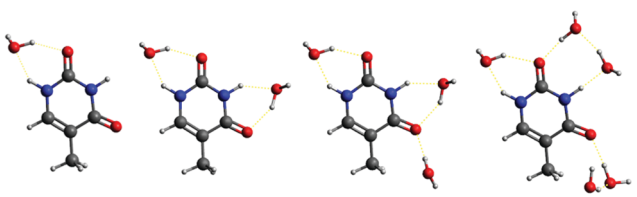

Fig. 7 Molecular structures of the thymine·water clusters (subset III) serving as tests for EFP-ADC.

Table 5 Vertical excitation energies and oscillator strengths of the five lowest excited singlet states of thymine in the gas phase (isolated) and the thymine·$n H_2O$ complexes at supermolecular ADC(3) level as well as with EFP-ADC(3). For the characterisation of the transition, 0 → 0 refers to HOMO → LUMO, −1 → +1 to HOMO−1 → LUMO+1, *etc.*

			Excitation energy (eV)		Oscillator strength	
Thymine·nH_2O	State	Transition	Super ADC(3)	EFP-ADC(3)	Super ADC(3)	EFP-ADC(3)
Isolated	S_1	−2 → 0	5.358	—	0.0001	—
	S_2	0 → 0	5.567	—	0.2295	—
	S_3	−1 → 0	6.797	—	0.0498	—
	S_4	−3 → +2	6.936	—	0.0000	—
	S_5	0 → +1	6.989	—	0.0000	—
$1H_2O$	S_1	−2 → 0	5.394	5.403	0.0001	0.0005
	S_2	0 → 0	5.524	5.499	0.2531	0.2339
	S_3	−1 → 0	6.909	6.881	0.0396	0.0340
	S_4	0 → +2	6.978	7.019	0.1890	0.2127
	S_5	−3 → +2	7.164	7.069	0.0001	0.0011
$2H_2O$	S_1	0 → 0	5.427	5.444	0.2341	0.2179
	S_2	−2 → 0	5.644	5.725	0.0001	0.0001
	S_3	−1 → 0	6.804	6.817	0.0444	0.0437
	S_4	0 → +2	6.966	7.001	0.2511	0.2533
	S_5	−3 → +2	7.123	7.189	0.0005	0.0002
$3H_2O$	S_1	0 → 0	5.311	5.354	0.2355	0.2063
	S_2	−2 → 0	5.813	5.912	0.0003	0.0001
	S_3	−1 → 0	6.771	6.821	0.0592	0.0507
	S_4	0 → +1	6.951	7.002	0.2986	0.3008
	S_5	−4 → +1	7.104	7.167	0.0001	0.0003
$5H_2O$	S_1	0 → 0	5.454	5.493	0.0010	0.0016
	S_2	−2 → 0	5.610	5.623	0.2481	0.2135
	S_3	0 → +1	6.712	6.797	0.1756	0.1717
	S_4	−1 → 0	6.971	6.974	0.1308	0.1075
	S_5	−5 → +1	7.473	7.578	0.0006	0.0002

Table 6 Vertical triplet excitation energies of thymine + nH$_2$O for EFP-ADC(3). For the characterisation of the transition, 0 → 0 refers to HOMO → LUMO, −1 → +1 to HOMO−1 → LUMO+1, *etc.*

	State	Transition	ADC(3)	EFP-ADC(3)
Isolated	T_1	0 → 0	3.669	—
	T_2	−2 → 0	5.086	—
	T_3	−1 → 0	5.400	—
	T_4	0 → +2	6.100	—
	T_5	−3 → +2	6.681	—
1H$_2$O	T_1	0 → 0	3.661	3.664
	T_2	−2 → 0	5.129	5.131
	T_3	−1 → 0	5.378	5.383
	T_4	0 → +2	6.095	6.101
	T_5	−3 → +2	6.797	6.830
2H$_2$O	T_1	0 → 0	3.682	3.682
	T_2	−1 → 0	5.340	5.347
	T_3	−2 → 0	5.386	5.468
	T_4	0 → +2	6.001	6.012
	T_5	−1 → +2	6.859	6.867
3H$_2$O	T_1	0 → 0	3.652	3.666
	T_2	0 → +1	5.325	5.346
	T_3	−2 → 0	5.570	5.670
	T_4	−1 → 0	5.917	5.952
	T_5	−4 → +1	6.865	6.927
5H$_2$O	T_1	0 → 0	3.675	3.687
	T_2	0 → +1	5.296	5.316
	T_3	−2 → 0	5.358	5.375
	T_4	−1 → 0	6.020	6.043
	T_5	−1 → +1	6.808	6.810

It is also interesting to realise that the mean absolute error in the solvation shifts stays practically constant with increasing number of water molecules from one to five with a value of 0.03 eV (Fig. 8, right), which is much smaller than the inherent error of the ADC(3) method.[30] In Fig. 8, it can be seen that the interaction strength of the solvent water molecules with thymine does indeed increase with the number of water molecules from −0.25 to almost +0.6 Hartree, and yet, the EFP approach is capable of capturing the solvent influence on the excited states (Table 7).

At the ADC(2) level, the agreement between supermolecular and EFP calculations is slightly worse (Fig. 8, left), but still good, as the error introduced through the EFP model is still much smaller than the inherent error of the ADC(2) excitation energies. Overall, the same trends hold for EFP-ADC(2) as observed for EFP-ADC(3) (see the ESI†).

5 Summary and conclusion

EFP-ADC(2) and EFP-ADC(3) have been introduced by combining two established methods: algebraic diagrammatic construction (ADC) methods for excitation energies and the effective fragment potential (EFP) approach as a polarisable environment model for solvation. These methods have been implemented into Q-Chem and extensively tested with respect to selected molecular solute·solvent complexes with different solvents and varying interaction strengths.

The overall accuracy of the EFP-ADC approaches has been found to be very high for singlet excitation energies with mean signed errors at the EFP-ADC(2) level of −0.042 ± 0.066 eV and −0.021 ± 0.057 eV at the EFP-ADC(3) level (Table 5). The mean absolute error for singlet excitation energies is slightly larger, 0.052 eV and 0.041 eV for EFP-ADC(2) and EFP-ADC(3), respectively, however, they are substantially smaller than the inherent errors in excitation energies of the parent ADC(2) and ADC(3) schemes. In general, EFP-ADC(3) outperforms EFP-ADC(2) owing to the smaller absolute errors and smaller standard deviations for singlet energy excitations. In general, triplet excitation energies have smaller errors at EFP-ADC(2) as well as EFP-ADC(3) levels with a mean absolute error of about 0.03 eV for both methods (Table 5). Oscillator strengths are generally very accurately

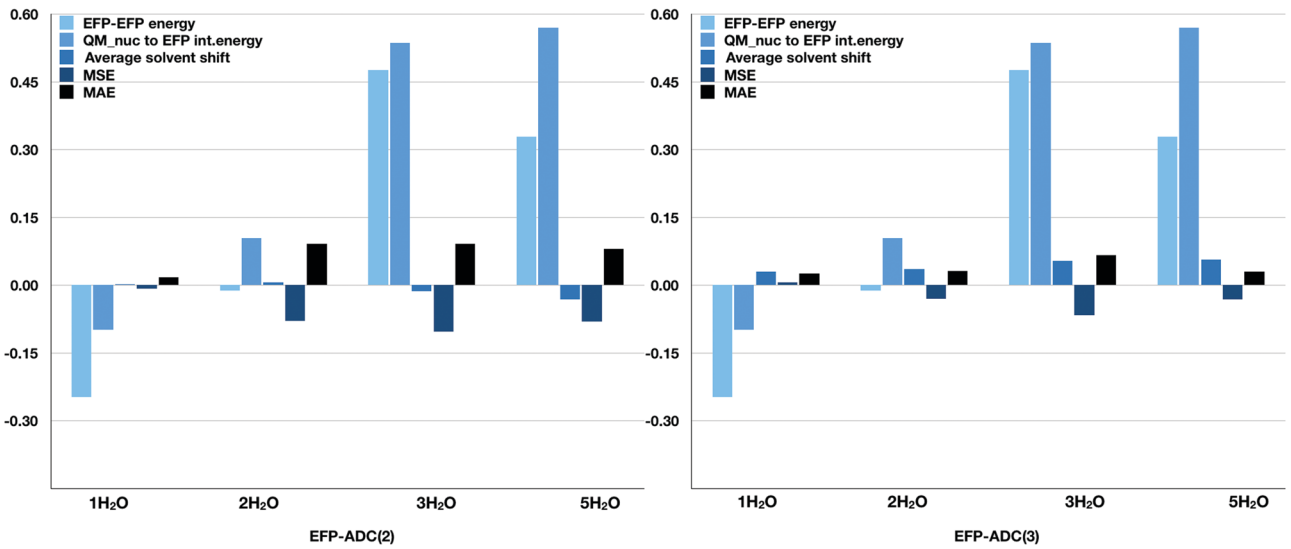

Fig. 8 EFP energy contributions with respect to the QM ground state in Hartree; MSE and MAE for triplet and singlet excitation energies in eV for the thymine·nH$_2$O complexes (n = 1, 2, 3, and 5) at the level of EFP-ADC(2) (left) and EFP-ADC(3) (right).

Table 7 Performance of EFP-ADC(2) and EFP-ADC(3)

	EFP-ADC(2)			EFP-ADC(3)		
	Singlet excitation energy	Oscillator strength	Triplet excitation energy	Singlet excitation energy	Oscillator strength	Triplet excitation energy
Count	80	79	80	55	53	55
MSE	−0.042	0.001	−0.024	−0.021	0.001	−0.013
Std deviation	0.066	0.024	0.050	0.057	0.011	0.045
MAE	0.052	0.013	0.033	0.041	0.005	0.029
Value with abs max $\|\Delta x\|$	−0.311	0.448	−0.163	−0.213	−0.036	−0.123

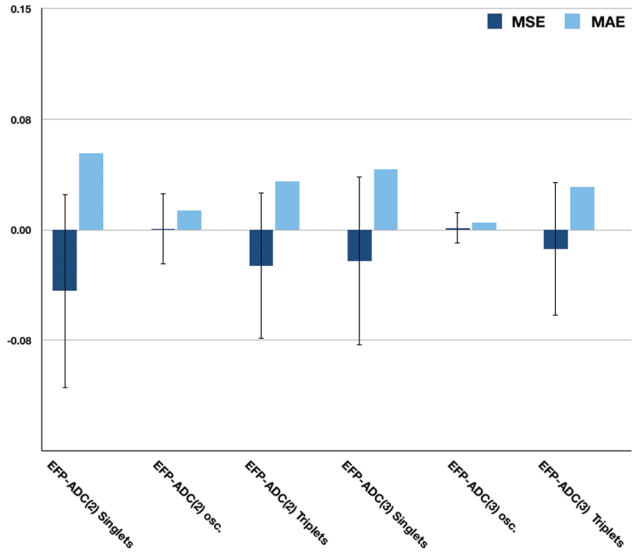

Fig. 9 Overall MAE and MSE comparison for the singlet excitation energies, corresponding oscillator strengths and triplet excitation energies for EFP-ADC(2) and EFP-ADC(3) along with standard deviation for MSE for all tested molecules of subsets I, II and III.

reproduced with errors of only 0.001 ± 0.013 and 0.001 ± 0.005 for EFP-ADC(2) and EFP-ADC(3), respectively. Outliers with larger errors occur when the molecular orbitals involved in the electronic transition are delocalised over the solvent molecule. For such situations, this solvent molecule needs to be included in the quantum region of the solute and not treated as an EFP fragment (Fig. 9).

A previous benchmark study of EFP-CCSD(T) using the S22 dataset for non-covalent interactions revealed a mean absolute error of 0.039 eV extrapolating the results to the complete basis set limit.[57] This agrees nicely with the results obtained for the EFP-ADC methods. However, at the moment, QM-EFP dispersion and exchange repulsion interactions are not yet implemented, therefore, the errors are expected to get even lower once these contributions are included. However, if the solvatochromic shifts are very small due to very weak solute–solvent interactions and lie below the numerical noise level of EFP-ADC of about 0.05 eV, as for solvated naphthalene, for example, EFP-ADC is not accurate enough to predict the solvent shifts correctly. Since the EFP-EFP interaction scales as N^2, simulations of systems with a very large number of solvent molecules, with a considerably smaller quantum system, will eventually be controlled by the EFP scaling. In general, EFP-ADC methods reproduce excitation energies and oscillator strengths with very good accuracy and are thus highly valuable in computing electronic absorption spectra of organic chromophores in solution.

Conflicts of interest

There are no conflicts to declare.

Acknowledgements

This work has been conducted within the Collaborative Research Center "N-heteropolycycles as functional materials" (SFB1249) of the German Science Foundation. Reena Sen received financial support from the Heidelberg graduate school, "Mathematical and Computational Methods in the Sciences" (GSC 220).

Notes and references

1 T. Helgaker, P. Jorgensen and J. Olsen, *Molecular Electronic-Structure Theory*, Wiley, Hoboken, 2014, p. 940.
2 J. Tomasi, B. Mennucci and R. Cammi, *Chem. Rev.*, 2005, **105**, 2999–3094.
3 B. Mennucci, *Wiley Interdiscip. Rev.: Comput. Mol. Sci.*, 2012, **2**, 386–404.
4 C. J. Cramer and D. G. Truhlar, *Acc. Chem. Res.*, 2008, **41**, 760–768.
5 A. Klamt and G. Schüürmann, *J. Chem. Soc., Perkin Trans. 2*, 1993, 799–805.
6 H. M. Senn and W. Thiel, *Angew. Chem., Int. Ed.*, 2009, **48**, 1198.
7 J. M. Olsen, K. Aidas and J. Kongsted, *J. Chem. Theory Comput.*, 2010, **6**, 3721–3734.
8 J. M. H. Olsen and J. Kongsted, *Adv. Quantum Chem.*, 2011, **61**, 107–143.
9 L. V. Slipchenko and M. S. Gordon, *J. Comput. Chem.*, 2007, **28**, 276–291.
10 M. S. Gordon, L. Slipchenko, H. Li and J. H. Jensen, *Annu. Rep. Comput. Chem.*, 2007, **3**, 177–193.
11 R. M. Richard and J. M. Herbert, *J. Chem. Phys.*, 2012, **137**, 064113.
12 R. M. Richard, K. U. Lao and J. M. Herbert, *Acc. Chem. Res.*, 2014, **47**, 2828–2836.
13 K. U. Lao and J. M. Herbert, *J. Phys. Chem. A*, 2015, **119**, 235–252.

14 P. N. Day, J. H. Jensen, M. S. Gordon, S. P. Webb, W. J. Stevens, M. Krauss, D. Garmer, H. Basch and D. Cohen, *J. Chem. Phys.*, 1996, **105**, 1968–1986.
15 M. S. Gordon, M. A. Freitag, P. Bandyopadhyay, J. H. Jensen, V. Kairys and W. J. Stevens, *J. Phys. Chem. A*, 2001, **105**, 293–307.
16 A. DeFusco, N. Minezawa, L. V. Slipchenko, F. Zahariev and M. S. Gordon, *J. Phys. Chem. Lett.*, 2011, **2**, 2184–2192.
17 L. V. Slipchenko, *J. Phys. Chem. A*, 2010, **114**, 8824–8830.
18 D. Kosenkov and L. V. Slipchenko, *J. Phys. Chem. A*, 2011, **115**, 392–401.
19 D. Ghosh, D. Kosenkov, V. Vanovschi, C. F. Williams, J. M. Herbert, M. S. Gordon, M. W. Schmidt, L. V. Slipchenko and A. I. Krylov, *J. Phys. Chem. A*, 2010, **114**, 12739–12754.
20 A. I. Krylov, *Annu. Rev. Phys. Chem.*, 2008, **59**, 433–462.
21 R. J. Bartlett, *Mol. Phys.*, 2010, **108**, 2905–2920.
22 K. Sneskov and O. Christiansen, *Wiley Interdiscip. Rev.: Comput. Mol. Sci.*, 2012, **2**, 566–584.
23 E. Runge and E. K. U. Gross, *Phys. Rev. Lett.*, 1984, **52**, 977–1000.
24 M. E. Casida, in *Recent Advances in Density Functional Methods Part I*, ed. D. P. Chong, World Scientific, Singapore, 1995, pp. 155–192.
25 A. Dreuw and M. Head-Gordon, *Chem. Rev.*, 2005, **105**, 4009–4037.
26 M. Head-Gordon, R. J. Rico, M. Oumi and T. J. Lee, *Chem. Phys. Lett.*, 1994, **219**, 21–29.
27 Y. M. Rhee and M. Head-Gordon, *J. Phys. Chem. A*, 2007, **111**, 5314–5326.
28 J. Schirmer, *Phys. Rev. A: At., Mol., Opt. Phys.*, 1982, **26**, 2395–2416.
29 A. B. Trofimov, G. Stelter and J. Schirmer, *J. Chem. Phys.*, 2002, **117**, 6402–6410.
30 P. H. P. Harbach, M. Wormit and A. Dreuw, *J. Chem. Phys.*, 2014, **141**, 064113.
31 M. Wormit, D. R. Rehn, P. H. Harbach, J. Wenzel, C. M. Krauter, E. Epifanovsky and A. Dreuw, *Mol. Phys.*, 2014, **112**, 774–784.
32 A. Dreuw and M. Wormit, *Wiley Interdiscip. Rev.: Comput. Mol. Sci.*, 2015, **5**, 82–95.
33 J. Schirmer and A. B. Trofimov, *J. Chem. Phys.*, 2004, **120**, 11449–11464.
34 A. P. Gamiz-Hernandez, I. N. Angelova, R. Send, D. Sundholm and V. R. I. Kaila, *Angew. Chem., Int. Ed.*, 2015, **54**, 11564–11566.
35 B. Lunkenheimer and A. Köhn, *J. Chem. Theory Comput.*, 2013, **9**, 977–994.
36 J.-M. Mewes, Z.-Q. You, M. Wormit, T. Kriesche, J. M. Herbert and A. Dreuw, *J. Phys. Chem. A*, 2015, **119**, 5446–5464.
37 J.-M. Mewes, J. M. Herbert and A. Dreuw, *Phys. Chem. Chem. Phys.*, 2017, **19**, 1644–1654.
38 M. Scheurer, M. F. Herbst, P. Reinholdt, J. M. H. Olsen, A. Dreuw and J. Kongsted, *J. Chem. Theory Comput.*, 2018, **14**, 4870–4883.
39 S. Prager, A. Zech, F. Aquilante, A. Dreuw and T. A. Wesolowski, *J. Chem. Phys.*, 2016, **144**, 204103.
40 S. Prager, A. Zech, T. A. Wesolowski and A. Dreuw, *J. Chem. Theory Comput.*, 2017, **13**, 4711–4725.
41 A. Zech, N. Ricardi, S. Prager, A. Dreuw and T. A. Wesolowski, *J. Chem. Theory Comput.*, 2018, **14**, 4028–4040.
42 J. Schirmer, *Many-Body Methods for Atoms, Molecules and Clusters*, Springer Berlin Heidelberg, 2018.
43 Y. Shao, Z. Gan, E. Epifanovsky, A. T. Gilbert, M. Wormit, J. Kussmann, A. W. Lange, A. Behn, J. Deng, X. Feng, D. Ghosh, M. Goldey, P. R. Horn, L. D. Jacobson, I. Kaliman, R. Z. Khaliullin, T. Kuś, A. Landau, J. Liu, E. I. Proynov, Y. M. Rhee, R. M. Richard, M. A. Rohrdanz, R. P. Steele, E. J. Sundstrom, H. L. Woodcock, P. M. Zimmerman, D. Zuev, B. Albrecht, E. Alguire, B. Austin, G. J. O. Beran, Y. A. Bernard, E. Berquist, K. Brandhorst, K. B. Bravaya, S. T. Brown, D. Casanova, C.-M. Chang, Y. Chen, S. H. Chien, K. D. Closser, D. L. Crittenden, M. Diedenhofen, R. A. DiStasio, H. Do, A. D. Dutoi, R. G. Edgar, S. Fatehi, L. Fusti-Molnar, A. Ghysels, A. Golubeva-Zadorozhnaya, J. Gomes, M. W. Hanson-Heine, P. H. Harbach, A. W. Hauser, E. G. Hohenstein, Z. C. Holden, T.-C. Jagau, H. Ji, B. Kaduk, K. Khistyaev, J. Kim, J. Kim, R. A. King, P. Klunzinger, D. Kosenkov, T. Kowalczyk, C. M. Krauter, K. U. Lao, A. D. Laurent, K. V. Lawler, S. V. Levchenko, C. Y. Lin, F. Liu, E. Livshits, R. C. Lochan, A. Luenser, P. Manohar, S. F. Manzer, S.-P. Mao, N. Mardirossian, A. V. Marenich, S. A. Maurer, N. J. Mayhall, E. Neuscamman, C. M. Oana, R. Olivares-Amaya, D. P. O'Neill, J. A. Parkhill, T. M. Perrine, R. Peverati, A. Prociuk, D. R. Rehn, E. Rosta, N. J. Russ, S. M. Sharada, S. Sharma, D. W. Small, A. Sodt, T. Stein, D. Stück, Y.-C. Su, A. J. Thom, T. Tsuchimochi, V. Vanovschi, L. Vogt, O. Vydrov, T. Wang, M. A. Watson, J. Wenzel, A. White, C. F. Williams, J. Yang, S. Yeganeh, S. R. Yost, Z.-Q. You, I. Y. Zhang, X. Zhang, Y. Zhao, B. R. Brooks, G. K. Chan, D. M. Chipman, C. J. Cramer, W. A. Goddard, M. S. Gordon, W. J. Hehre, A. Klamt, H. F. Schaefer, M. W. Schmidt, C. D. Sherrill, D. G. Truhlar, A. Warshel, X. Xu, A. Aspuru-Guzik, R. Baer, A. T. Bell, N. A. Besley, J.-D. Chai, A. Dreuw, B. D. Dunietz, T. R. Furlani, S. R. Gwaltney, C.-P. Hsu, Y. Jung, J. Kong, D. S. Lambrecht, W. Liang, C. Ochsenfeld, V. A. Rassolov, L. V. Slipchenko, J. E. Subotnik, T. Van Voorhis, J. M. Herbert, A. I. Krylov, P. M. Gill and M. Head-Gordon, *Mol. Phys.*, 2015, **113**, 184–215.
44 A. Trofimov, I. Krivdina, J. Weller and J. Schirmer, *Chem. Phys.*, 2006, **329**, 1–10.
45 M. Caricato, B. Mennucci and J. Tomasi, *J. Chem. Phys.*, 2006, **124**, 124520.
46 J. Wenzel, M. Wormit and A. Dreuw, *J. Comput. Chem.*, 2014, **35**, 1900–1915.
47 J. Wenzel, M. Wormit and A. Dreuw, *J. Chem. Theory Comput.*, 2014, **10**, 4583–4598.
48 J. Wenzel, A. Holzer, M. Wormit and A. Dreuw, *J. Chem. Phys.*, 2015, **142**, 214104.
49 C. M. Krauter, M. Pernpointner and A. Dreuw, *J. Chem. Phys.*, 2013, **138**, 044107.

50 D. Lefrancois, M. Wormit and A. Dreuw, *J. Chem. Phys.*, 2015, **143**, 124107.
51 D. Lefrancois, D. R. Rehn and A. Dreuw, *J. Chem. Phys.*, 2016, **145**, 084102.
52 C. M. Krauter, B. Schimmelpfennig, M. Pernpointner and A. Dreuw, *Chem. Phys.*, 2017, **482**, 286–293.
53 S. Knippenberg, D. R. Rehn, M. Wormit, J. H. Starcke, I. L. Rusakova, A. B. Trofimov and A. Dreuw, *J. Chem. Phys.*, 2012, **136**, 064107.
54 F. Plasser, M. Wormit and A. Dreuw, *J. Chem. Phys.*, 2014, **141**, 024106.
55 F. Plasser, S. A. Bäppler, M. Wormit and A. Dreuw, *J. Chem. Phys.*, 2014, **141**, 024107.
56 S. A. Bäppler, F. Plasser, M. Wormit and A. Dreuw, *Phys. Rev. A: At., Mol., Opt. Phys.*, 2014, **90**, 052521.
57 J. C. Flick, D. Kosenkov, E. G. Hohenstein, C. D. Sherrill and L. V. Slipchenko, *J. Chem. Theory Comput.*, 2012, **8**, 2835–2843.

